AGU PUBLICATIONS

Geophysical Research Letters

RESEARCH LETTER
10.1002/2015GL063869

Key Points:
- Mantle scattering cannot be linked to one type of heterogeneity
- The inner core strongly influences the *PKP* precursor/*PKIKP* amplitude ratios
- There is no correlation between scattering and long-scale CMB velocity structure

Supporting Information:
- Tables S1 and S2 and Figures S1–S11

Correspondence to:
L. Waszek,
lw313@cam.ac.uk

Citation:
Waszek, L., C. Thomas, and A. Deuss (2015), *PKP* precursors: Implications for global scatterers, *Geophys. Res. Lett.*, *42*, 3829–3838, doi:10.1002/2015GL063869.

Received 16 MAR 2015
Accepted 25 APR 2015
Accepted article online 2 MAY 2015
Published online 26 MAY 2015

PKP precursors: Implications for global scatterers

Lauren Waszek[1], Christine Thomas[2], and Arwen Deuss[3]

[1]Bullard Laboratories, University of Cambridge, Cambridge, UK, [2]Institut für Geophysik, Münster, Germany, [3]Department of Earth Sciences, Utrecht University, Utrecht, Netherlands

Abstract Precursors to the core phase *PKP* are generated by scattering of seismic energy from heterogeneities in the mantle. Here we examine a large global data set of *PKP* precursors in individual seismograms and array data, to better understand scattering locations. The precursor amplitudes from individual seismograms are analyzed with respect to the inner core phase *PKIKP* and mantle phase *PP*. We find and correct for a hemispherical asymmetry in the precursor/*PKIKP* amplitudes, resulting from inner core structure. Using ray tracing, we locate scatterers in our array data and use these to infer scattering locations in the individual data. The scattering strength displays regional variation; however, we find no relationship with long-scale core-mantle boundary velocity structure. Scattering is observed in all regions of data coverage, as are paths with no precursors. This indicates that scattering occurs from various small-scale heterogeneities, including but not limited to ultralow velocity zones or partial melt, and slabs.

1. Introduction

As the strongest thermochemical discontinuity in the Earth, separating the silicate mantle and metallic core, the core-mantle boundary (CMB) is of great geodynamical interest. The approximately 300 km thick *D″* layer above the CMB is highly complex, displaying large variations in velocity and attenuation structures [*Garnero*, 2000]. Strong compositional and thermal heterogeneities arise from structures such as subducting slabs, large low shear velocity provinces (LLSVPs), ultralow velocity zones (ULVZs), and CMB topography [*Garnero et al.*, 1998; *Sze and van der Hilst*, 2003; *Ritsema et al.*, 2004; *McNamara et al.*, 2010; *Koelemeijer et al.*, 2012]. Constraining the properties in this region is important for understanding processes in the mantle, and the interaction between mantle and core. However, these structures have not yet been fully mapped, and their relationship to the mechanisms at the CMB is not understood.

Mantle heterogeneity causes scattering of seismic energy, which is observed as precursors to the core phase *PKP* [*Cleary and Haddon*, 1972; *Doornbos and Husebye*, 1972]. Although scattering occurs throughout the mantle [*Hedlin et al.*, 1997; *Margerin and Nolet*, 2003; *Kaneshima and Helffrich*, 2009; *Mancinelli and Shearer*, 2013], the largest-amplitude precursors are generated from greater velocity differences near the CMB [*Haddon and Cleary*, 1973; *Vidale and Hedlin*, 1998; *Wen and Helmberger*, 1998; *Thomas et al.*, 1999, 2009]. The primary source of this scattering remains unclear. The scatter shows much lateral variation, indicating changes on small length scales (< 50 km) [*Hedlin and Shearer*, 2000]. The strongest scatterers have been linked to sharp velocity transitions, such as regions of partial melt [*Wen*, 2000], heterogeneities in deep subducted slabs [*Cao and Romanowicz*, 2007; *Miller and Niu*, 2008; *Vanacore et al.*, 2010], and topography of the CMB [*Doornbos*, 1978]. Regional variations in precursor amplitudes have also been observed [*Hedlin and Shearer*, 2000], with stronger scattering beneath North America, Africa, and India and weaker scattering beneath South and Central America, Europe, and Indonesia. However, a clear relationship between these regional differences and seismic structures in the mantle has not been determined, in part due to limited resolution of mantle models.

Previous studies have considered the precursor amplitudes and arrival times relative to the inner core phase *PKIKP* [e.g., *Doornbos and Husebye*, 1972; *Hedlin et al.*, 1997; *Niu and Wen*, 2001]. However, the upper inner core displays a hemispherical asymmetry in seismic properties, whereby the west hemisphere has stronger velocity anisotropy, lower seismic velocity, and weaker attenuation [*Tanaka and Hamaguchi*, 1997; *Deuss et al.*, 2010; *Waszek and Deuss*, 2011, 2013]. The combination of these structures results in a hemispherical difference in the amplitude and arrival time of *PKIKP*. Waves which travel through the west hemisphere arrive later and with a larger amplitude than those which traverse the east [e.g., *Waszek and Deuss*, 2013]. We investigate the effects of inner core structure on the precursor/*PKIKP* amplitude ratios and apply corrections before further

analysis. Without these corrections, the hemispherical variation in the inner core has a significant influence on the precursor/*PKIKP* amplitude ratios.

Although precursors are detected in individual seismograms, the location of scatterers cannot be determined as there is no information regarding incoming angle. In particular, it is not possible to distinguish between scattering on the receiver and source sides [*Hedlin and Shearer*, 2000]. However, data from seismic arrays contain slowness resolution, and so the location of the scatterer can be calculated [*Thomas et al.*, 1999]. We use array data to constrain the location of scatterers in the lower mantle. Subsequently, we compare the confirmed scatterer locations with the mantle paths of individual seismograms to map probable scatterer locations and their strength in the individual data.

We seek to improve on global observations of scattering strength in order to understand the structures which generate scatter. We search for *PKP* precursors in a large high-quality global *PKIKP* data set of individual seismograms and array data, which was originally collected to study the inner core [*Waszek et al.*, 2011]. For the individual seismograms, we examine the amplitudes of the precursors with respect to *PKIKP* and *PP*. We remove the effects of inner core structure for individual seismograms and locate scatterers in the array data using ray tracing methods. Finally, we search for any correlation between scattering strength and lower mantle velocity structures.

2. Data and Processing

PKP precursors are generated by scattering in the lower mantle. They travel through the outer core and are detected as arrivals preceding the inner core phase *PKIKP* by up to 60 s [*Cleary and Haddon*, 1972; *Hedlin et al.*, 1997]. Scattering may occur on both source and receiver sides, and scattered waves on the receiver side traverse the outer core along *PKP* paths. We search for precursors in an updated version of the *PKIKP-PKiKP* data set compiled by *Waszek et al.* [2011], using events from January 1990 to December 2013 with magnitude $5.3 \leq M_w \leq 6.4$ and depth ≥ 15 km. For reference phases, we use *PKIKP* and the mantle phase *PP*. The initial data set comprises over 40,000 individual seismograms in the distance range of 130–143°, with 1406 events observed at arrays. For our quality checks, we require that *PKIKP* can be clearly visible. This corresponds to 3184 individual seismograms and 176 array stacks.

As precursors vary in frequency, we test several different band-pass filters in the range 0.1–3.0 Hz for the individual seismograms and array data. Our preferred filter to observe the *PKP* precursors is between 0.7 and 2.0 Hz. This also centers on the main frequency of *PKIKP* and removes lower frequency diffracted energy from the *PKP-b* caustic [*Thomas et al.*, 2009]. Figure 1a shows examples of seismograms with and without precursors. In the first trace, precursors are observed as the smaller-amplitude signals preceding *PKIKP* by 11 s. Using the Seismic Analysis Code [*Goldstein et al.*, 2003] used for manipulation of seismograms, we measure the amplitude of the earliest precursor arrival, in addition to the maximum amplitude in the precursor window (Figures 1a and S1 in the supporting information). For comparison, we measure the *PKIKP* and *PP* signal amplitudes (Figure S1). No precursors are observed in the second trace.

We define arrays as more than seven stations within a maximum distance of 6° and maximum azimuth difference of 15°. This means that we also benefit from stations in dense regional networks. The arrays and networks used are listed in Table S1. We generate vespagrams for each event-array combination using fourth-power phase-weighted stacking [*Schimmel and Paulssen*, 1997]. Prior to stacking, the traces are normalized and aligned on *PKIKP*. Examples of vespagrams are presented in Figure 1b. The first vespagram shows several precursors arriving 25–15 s before *PKIKP*, with slowness 0.5–2.5 s per degree higher. The second vespagram shows no precursors. We measure the precursor-*PKIKP* travel time and slowness differentials for every observed precursor signal.

Since the phase weighting artificially amplifies coherent signals, direct amplitude measurements for the array data vespagrams would be misleading. Additionally, incoherent precursor arrivals will not stack in the vespagrams; thus, precursor strength is not wholly indicative of scattering strength. Instead, we classify our precursor strength with respect to the *PKIKP* and *PP* signals in the vespagrams. "Strong" is a precursor amplitude comparable to *PKIKP* and *PP*, whereas "weak" indicates that the reference signals dominate.

In order to locate the scatterers in the array data, we perform a grid search for hypothetical scatterer locations in the lower mantle. The grids are centered on the theoretical CMB entry and exit points of the *PKIKP* ray, of size 30° by 30° and spacing 1°, at depths every 50 km up to 500 km above the CMB. We center on the *PKIKP*

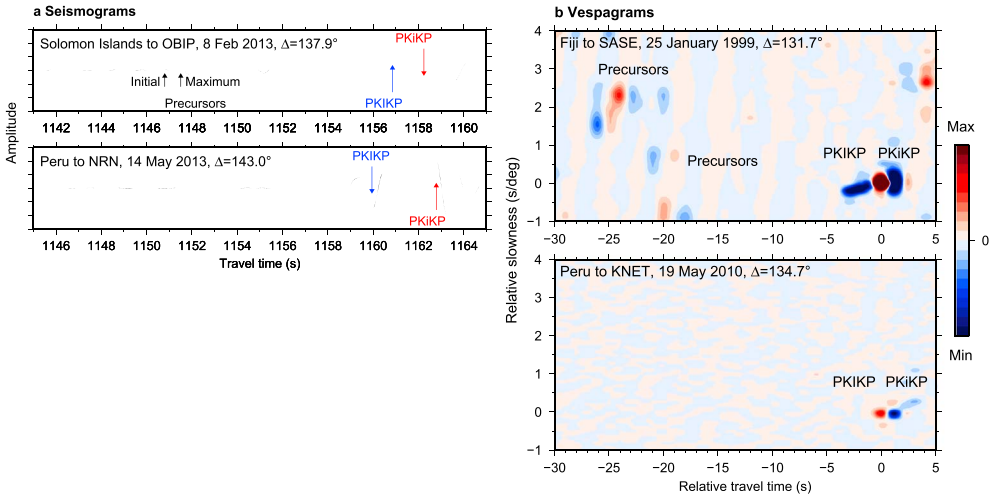

Figure 1. Examples of data with and without visible *PKP* precursors. (a) Individual seismograms. (b) Vespagrams aligned on *PKIKP*, stacking 14 seismograms for the Fiji event and 11 for the Peru event.

entry and exit points as this is our reference phase from which we calculate differential time and slowness. However, the precursors may also arise from scattered *PKPbc* phases, which is taken into account by our large search area. We simulate scattering by combining *P* and *PKP* raypaths to model *PKP* precursor paths (corresponding to single scattering) and use TauP [*Crotwell et al.*, 1999] to calculate theoretical paths between the scattering point and the event and station locations. This gives an estimate of the travel time and slowness of *PKP* precursors scattered from each grid point. We then minimize the theoretical precursor-*PKIKP* travel time and slowness differentials with respect to our observations to determine the most likely scattering location.

3. Observations

3.1. *PKP* Precursors

We present the geographic distribution of our observations of *PKP* precursors in individual seismograms in Figure 2a. Figure S2 shows the data as a function of *PKIKP* turning longitude. Individual paths with visible precursors are found in all areas of data coverage and display large variations in amplitude (Figures 2a). The number of seismograms with observed precursors decreases at larger epicentral distances (Figure S3a), in good agreement with previous studies [*Hedlin and Shearer*, 2000]. Figure S4 shows the data coverage at the CMB for all individual seismograms used in this study, both with and without PKP precursors. We note that we have very limited coverage in the center of the LLSVPs.

Seismograms with no visible precursors are also found globally (Figure 2b). These data have very similar raypaths to seismograms with large-amplitude precursors, which may indicate small length scales of scattering structures. However, the lack of detection does not mean that there is no scattering along these paths. The precursors may be smaller than the noise levels or removed by our filter if the frequency is significantly different to *PKIKP*. We find that the number of seismograms with no precursors decreases as a function of epicentral distance (Figure S3b). This is probably a result of removing ambiguous seismograms, as the precursors become larger and difficult to distinguish from the main *PKIKP* phase with increasing distance [*Hedlin and Shearer*, 2000].

The array data are presented in Figure 2c. Paths with strong precursors are observed globally; however, some regional variation is evident. There is a higher proportion of paths with strong precursors originating from events in the southwest Pacific and southeast Asia regions. Conversely, there are fewer strong precursors from events in South America and the South Sandwich Islands. As above, paths with no precursors are also observed in all areas of data coverage. This does not necessarily mean that there are no scatterers along these paths, since only coherent energy is visible in vespagrams. Incoherent precursors may arise from any differences between array stations; for example, mantle and crust structure, or multiple scatterers. These precursors will not be detected in vespagrams but may be observed in single traces. Hence, a comparison between the array data and individual data is required.

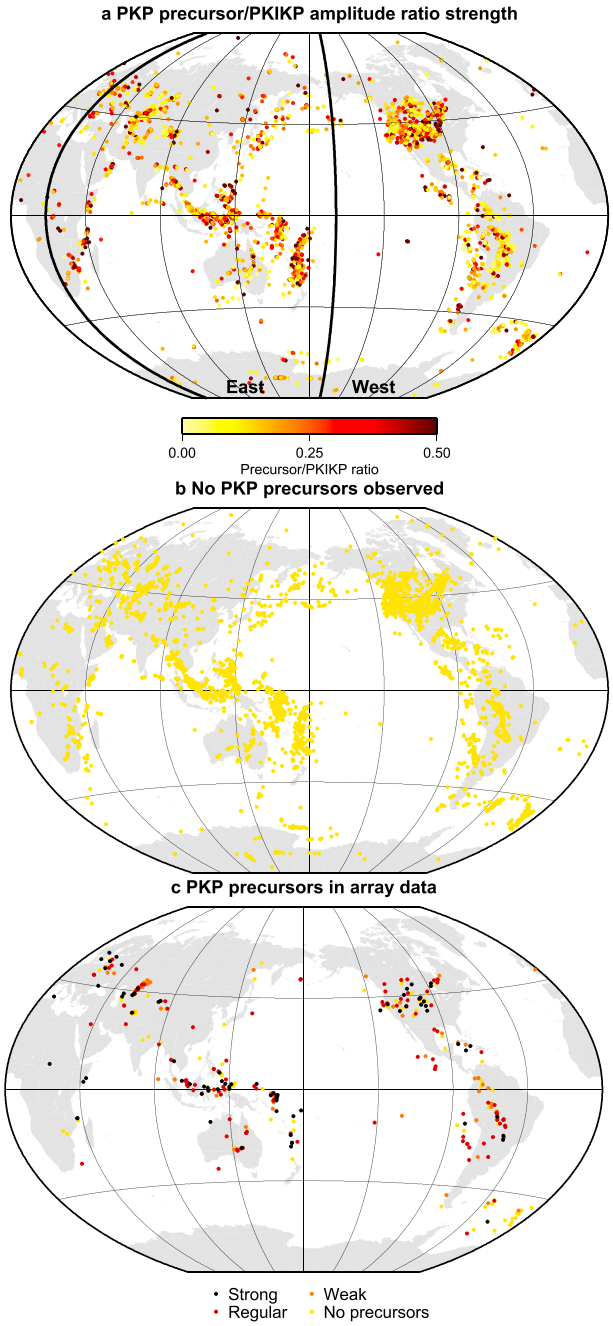

Figure 2. Maps showing locations of precursor observations in individual seismograms and array data. The circles correspond to CMB entry and exit points of *PKIKP*. Inner core hemisphere boundaries are shown. (a) Individual seismograms with *PKP* precursors. The color of the circles corresponds to the earliest arriving precursor/*PKIKP* amplitude ratio. (b) Individual seismograms with no precursors. (c) Array data. Colors correspond to precursor strength with respect to *PKIKP*.

3.2. Corrections for Inner Core Structure

In order to examine and correct for the influence of hemispherical structure on our reference phase *PKIKP*, we partition the data into east and west hemispheres according to *PKIKP* turning longitude. We use the hemisphere boundaries determined by *Waszek et al.* [2011] (Figure 2a). The data are further partitioned into three epicentral distance ranges (130–134°, 134–138.5°, and 138.5–143°) (Figure 3). These correspond to the depth layers of the hemispherical velocity and attenuation models we use to correct the *PKIKP* amplitudes [*Waszek and Deuss*, 2011, 2013]. For the depth layers, we calculate average precursor/*PKIKP* amplitude ratios in each

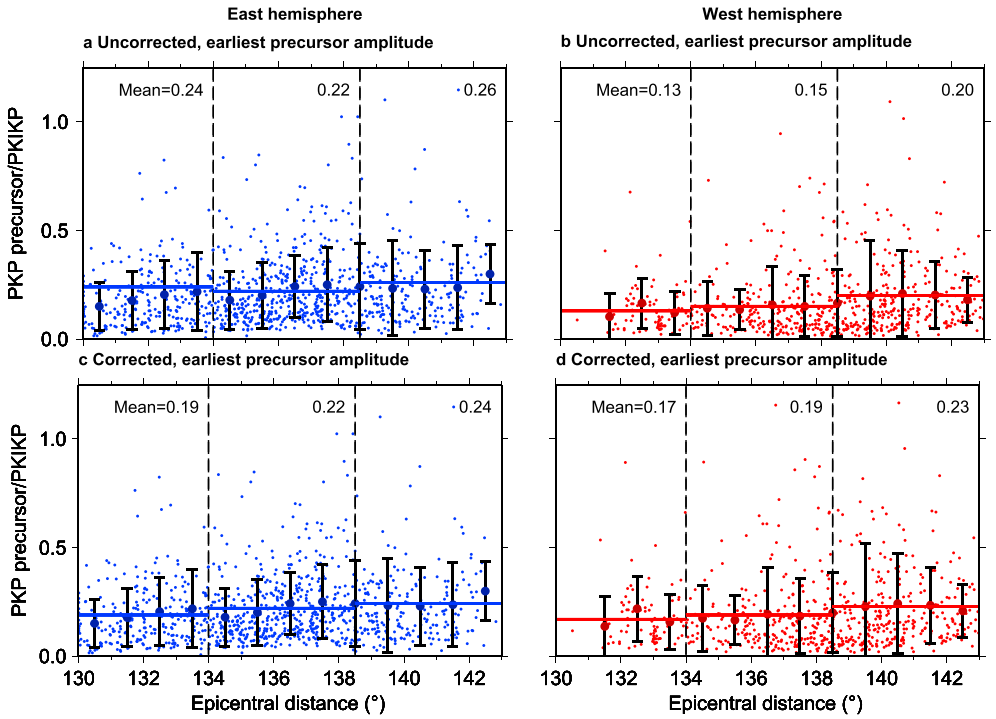

Figure 3. Earliest *PKP* precursor/*PKIKP* amplitude ratios as a function of epicentral distance. The data are partitioned into hemispheres by *PKIKP* turning longitude. Mean values are included for the distance ranges. (a, b) Uncorrected data. (c, d) *PKIKP* amplitude corrected for inner core velocity and attenuation structure.

hemisphere and perform a *t* test on the averages to determine the statistical significance of their differences. The *t* test is a statistical test used to determine whether two data sets are statistically different, even if the difference is small. We also calculate average amplitude ratios for precursor/*PP* and *PKIKP*/*PP* data, for comparison with mantle paths. The results are summarized in Table S2.

The average earliest precursor/*PKIKP* amplitude ratio is 0.23 in the east hemisphere and 0.17 in the west (Figures 3a, 3b, and S2a). The maximum precursor/*PKIKP* amplitude ratios are 0.47 and 0.38, respectively (Figures S2b, S5a, and S5b). The hemispherical differences are significant at the 1% level, which means that the probability that there is no difference between the hemispheres is less than 1% . A higher-amplitude ratio corresponds to a larger precursor, or smaller *PKIKP*. To determine which phase is influenced by the hemispherical difference, we examine the precursor/*PP* amplitude data (Figure S2c). There is no statistically significant difference in these data. We also find no hemispherical difference in the earliest/maximum precursor amplitude (Table S2). Conversely, the *PKIKP*/*PP* data display a hemispherical difference, which is significant at the 1% level (Figure S2d). Hence, the hemispherical variation in the precursor/*PKIKP* data arises from *PKIKP* and the inner core structure. This is expected, since the scattering locations of the precursors are not related to the *PKIKP* hemisphere.

Waszek and Deuss [2013] determined that the *PKIKP* phase is approximately 1.30 times larger in the west hemisphere due to the different velocity and attenuation structures. Our precursor/*PKIKP* amplitude ratios are on average 1.30 times larger in the east hemisphere, in excellent agreement. We correct our results using average theoretical *PKIKP* amplitudes calculated for isotropic hemispherical velocity and attenuation models for the three depth layers [*Waszek and Deuss*, 2011, 2013]. After correction, the average amplitude ratios are 0.22 and 0.20 in the east and west hemispheres, respectively, for the earliest precursor amplitude (Figures 3c and 3d) and 0.44 and 0.46 for the earliest precursor amplitude (Figures S5c and S5d). There is no statistically significant difference between either of the corrected data sets. Although this correction removes the average hemispherical difference, it does not change the variation of the *PKIKP* amplitudes within the hemispheres, arising from regional inner core structure.

3.3. Mapping Strength of Scattering

The scatterer locations constrained from our array data are shown in Figures 4a and S6. Figure S7 contains *PKIKP* core pierce points for array data with no precursors. We find evidence for some regional variation in location of scatters. There is a high proportion of scatterers beneath northern North America and western South America, whereas paths with no scatterers are found beneath southern Africa, the south Atlantic, and central North America. We observe much variation in precursor strength within regions in which scatters are located, such as beneath Southeast Asia and the south Pacific. Paths without precursors are found in close proximity to observed scatterers (less than 100 km).

We use the *PKIKP* core entry and exit points of the individual seismograms (Figure 2a) to generate maps of the earliest precursor/*PKIKP* amplitude ratios, corrected for hemispherical structure in the inner core (Figures 4b and S8), and taking averages in 2.5° bins. Although we cannot locate scatterers from individual seismograms, we compare locations of scatterers in array data (Figures 4a and S6) with the CMB pierce points of our individual data (Figures 4b and S8) to determine where scattering is most likely to have occurred. For this, we assume that scatterers on either the source or receiver sides of the CMB can result in *PKP* precursors. We keep only individual data which have CMB pierce points within 10° of located scatterers on either the source or receiver sides, which helps to decrease some uncertainty in scatterer location and remove data from areas where we have no constraints. These data are presented in Figures 4c and S9.

Comparing Figures 4a and 4c, we find that scattering is observed in all areas of data coverage, including regions which also contain paths with no precursors. Strong variation on small length scales is apparent in the individual data, in agreement with earlier studies [*Hedlin and Shearer*, 2000; *Vanacore et al.*, 2010]. This may be due in part to the limited constraints on scatterer location for the individual seismograms, as we only have knowledge of the *PKIKP* raypath and not the precursor raypath. Although we have some constraints on scatterer locations using our array grid search, which may be improved upon with migration methods, it is not possible to map these precisely to the individual data. We again find much overlap between the regions with scatterers and raypaths with no observable *PKP* precursors (Figure 2b).

We compare our scattering strength observations to the *P* wave model MITP08 [*Li et al.*, 2008] in the lower mantle. Scattering has previously been detected from locations with strong velocity transitions [*Wen and Helmberger*, 1998; *Niu and Wen*, 2001; *Cao and Romanowicz*, 2007; *Miller and Niu*, 2008; *Thomas et al.*, 2009]. However, we do not find consistent correlation between scattering strength and lateral velocity gradients. Furthermore, locations of data with no scattering appear unrelated to the velocity models (Figures 2b and S7). The limited resolution of tomography models means that it is difficult to attribute scattering to specific velocity variations. Smaller-scale structures such as ULVZs and slabs have been observed to generate large-amplitude *PKP* precursors [*Wen and Helmberger*, 1998; *Thomas et al.*, 2009; *Vanacore et al.*, 2010; *Sigloch and Mihalnyuk*, 2013]. However, we find no relationship between the strength of scatterers and a map of ULVZs [*McNamara et al.*, 2010] nor any other *D*′′ features. Indeed, we observe scattering in almost every region that we have data coverage, and large variability within these regions. This suggests that scattering occurs on much shorter length scales than the CMB structures.

The distance between a located scatterer and an array path with no precursors indicates a maximum scatterer length scale as less than ~100 km. This result is limited by the relatively few array data, however. Thus, we also compare the scatterer locations to the CMB pierce points of individual data with no precursors, determining a minimum separation of 60 km. For the individual data, we find a separation of 12 km between the CMB pierce points of a seismogram with precursors and a seismogram without. These observations provide strong evidence that the length scale of scatterers is smaller than the structures at the CMB, in excellent agreement with *Hedlin and Shearer* [2000]. Furthermore, our result indicates that we would not expect to detect a spatial correlation with the larger-scale features in the lower mantle.

In our array data, several of the observed *PKP* precursors cannot be located by our grid search, and hence, they are probably not produced by single scattering in the lower mantle (Figure S10). These paths may be explained by multiple scattering, which is difficult to constrain using ray tracing technique due to large errors. Comparing Figure 2c with Figure 4a, we find several instances where scatterers are observed at both the CMB entry and exit points of our rays, such as from the southwest Pacific to Europe and from Southeast Asia to North America. This corresponds extremely well to the majority of paths in which we observe unexplained precursors (Figure S10). Alternatively, the scattering may occur from other parts of the Earth, such as the uppermost

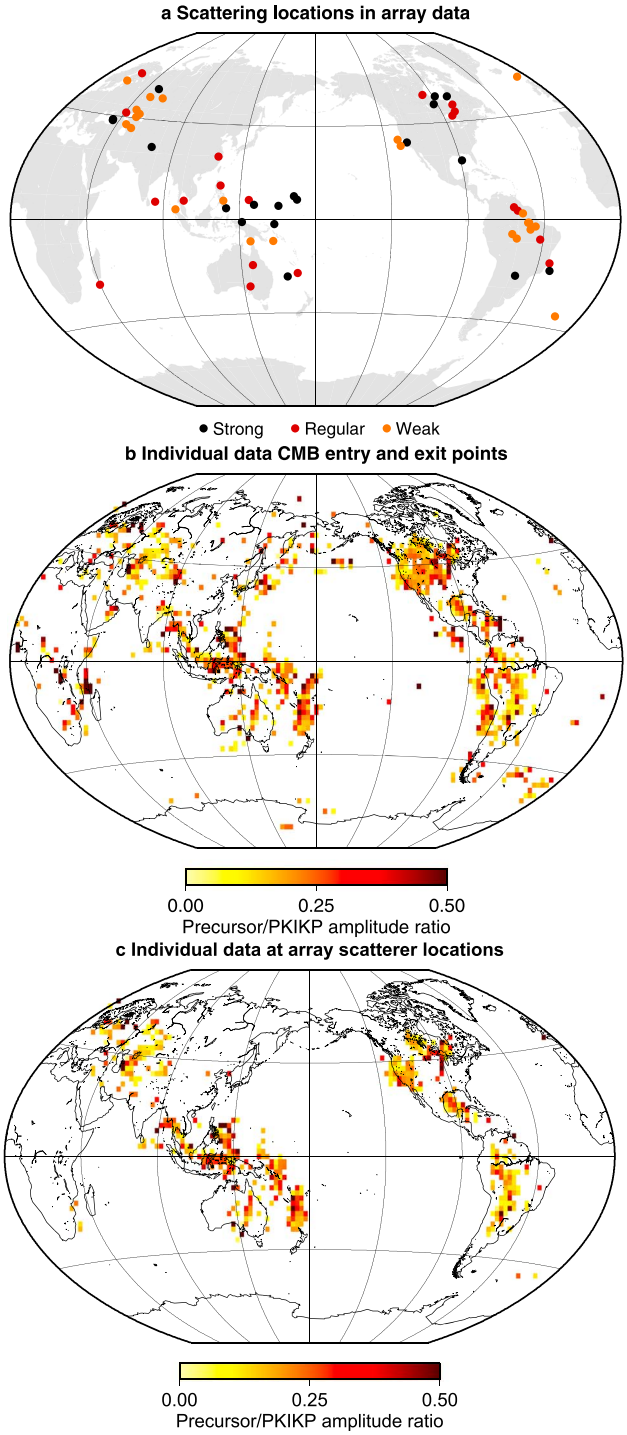

Figure 4. (a) Locations of scatterers in the mantle, calculated from array data. (b) Earliest precursor/*PKIKP* amplitude ratios corrected for inner core structure for the individual seismograms, generated using CMB entry and exit points of the *PKIKP* paths, for averages in 2.5° bins. (c) Corrected earliest precursor/*PKIKP* amplitude ratios for the individual seismograms, generated for CMB pierce points which are within 10° of scatterers located in array data, for averages in 2.5° bins. Colors correspond to precursor strength with respect to *PKIKP*.

inner core [*Thomas et al.*, 1999; *Cormier*, 2007]. Further modeling is required to determine the likely origin of this scattering.

We present examples of our grid search analysis misfits in Figure S11. The lateral resolution of our grid is 1°, a maximum distance of 60 km at the CMB, and vertical resolution is 50 km. We consider misfit of travel time and slowness to locate the scatterers. Errors in our results may arise from the effect of 3-D mantle structure versus a 1-D reference Earth model and random noise affecting our measurements. Thus, we allow a maximum difference of $\pm$1.0 s and $\pm$0.2 s per degree between our observed and theoretical values and locate the scatterer at the position which minimizes both values (Figure S11a). However, if the observed and theoretical results are very different, then we cannot locate the scatterer (Figure S11b).

4. Discussion

We observe a significant hemispherical difference in our precursor/*PKIKP* amplitude ratio data, which results from the influence of inner core velocity and attenuation structure on the *PKIKP* amplitude [*Wen and Niu*, 2002; *Waszek and Deuss*, 2013]. We correct for the hemispherical variation; however, regional structure within each hemisphere and anisotropy in the inner core may still affect the *PKIKP* amplitudes. Structure at the Inner core boundary (ICB) and within the inner core may also cause scatter in the precursor/*PKIKP* amplitude ratio data. Thus, the actual scattering strength may be smaller or larger than the data suggest and care must be taken when investigating and interpreting regional variations.

Discrepancies also arise from the path difference of the *PKP* precursors and *PKIKP*. Attenuation in the mantle and variation in velocity and density contrast at the CMB will strongly affect the signal amplitudes. This is particularly problematic for our analysis of the individual seismograms. Since we do not have constraints on the *PKP* precursor raypaths [*Hedlin and Shearer*, 2000], we use the *PKIKP* raypath to map the precursor scattering strength at the CMB. This introduces errors into Figure 4c, observed as the large variability in the precursor/*PKIKP* amplitude ratios.

We find no evidence for a correlation between precursor strength and long-scale CMB velocity structure nor with regions of strong lateral velocity gradient. This may be in part due to the limited resolution of the seismic velocity models. Instead, we suggest that scattering occurs from heterogeneities on the order of tens of kilometers, which are not resolved in global tomographic maps. Additionally, the scattering cannot be attributed to just one type of heterogeneity. The scattering locations correspond to various smaller-scale structures in the lower mantle, such as ULVZs or partial melt, and ancient slabs [*Cao and Romanowicz*, 2007; *Miller and Niu*, 2008; *Thomas et al.*, 2009; *McNamara et al.*, 2010; *Vanacore et al.*, 2010; *Sigloch and Mihalnyuk*, 2013] but also arise from other regions. The scattering strength does not appear to depend on the type of scatterer, either. Thus, further investigation is required into the strength of scattering from known features to understand the large variability in amplitude.

In order to explain our results, scattering must be generated by heterogeneities present throughout the mantle [*Christensen and Hofmann*, 1994; *Brandenburg and van Keken*, 2007], in addition to CMB topography [*Doornbos*, 1978], shallower mantle structure [*Margerin and Nolet*, 2003; *Mancinelli and Shearer*, 2013], and small-scale structure in the upper inner core [*Cormier*, 2007; *Yee et al.*, 2014]. It seems likely that scattering is also generated from heterogeneities present within regions which do not show strong lateral velocity contrasts, in good agreement with our estimates of small length scale scatterers. Multiple scattering must also be considered. This is corroborated by our precursor observations which cannot be explained by single lower mantle scattering (Figure S10). The next step is to investigate how the precursors vary depending on the location of the scatterers and the relationship to the type of scattering structure.

5. Conclusions

We observe a hemispherical asymmetry in the travel time and amplitudes of *PKP* precursors with respect to *PKIKP*, as a result of inner core structure. Inner core velocity and attenuation models are used to correct for this difference; however, regional inner core variations may still affect the corrected data. We constrain scatterer locations and strength using ray tracing methods for the array data and use these to infer likely scattering locations in the individual seismograms. There is no evidence of any correlation between precursor strength and long-scale velocity structure at the CMB from tomographic models. Instead, scattering is observed from throughout the lower mantle, in all regions of data coverage. Paths with no precursors are also observed

globally. This indicates that scattering structures must be small scale, and scattering is generated by multiple different types of heterogeneity, including ULVZs or partial melt and slabs. Additional, unconstrained structures are also likely to generate scatter. Further work into the relationship between the precursors and the type of scatterers is required.

Acknowledgments

L.W. is funded by a Research Fellowship from Homerton College, Cambridge. A.D. is funded by the European Research Council under the European Community's Seventh Framework Programme (FP7/2007-2013)/ERC grant 204995 and by a Philip Leverhulme Prize. We thank two anonymous reviewers for their helpful and constructive comments. The facilities of the IRIS Data Management System, and specifically the IRIS Data Management Center, were used for access to waveform and metadata required in this study. The IRIS DMS is funded through the National Science Foundation and specifically the GEO Directorate through the Instrumentation and Facilities Program of the National Science Foundation under cooperative agreement EAR-1063471 (http://www.iris.edu/wilber3/). All data are available from IRIS, and the original data set from which our data is taken was first published in *Waszek et al.* [2011].

The Editor thanks two anonymous reviewers for their assistance in evaluating this paper.

References

Brandenburg, J. P., and P. E. van Keken (2007), Deep storage of oceanic crust in a vigorously convecting mantle, *J. Geophys. Res.*, *112*, B06403, doi:10.1029/2006JB004813.

Cao, A., and B. Romanowicz (2007), Locating scatterers in the mantle using array analysis of PKP precursors from an earthquake doublet, *Earth Planet. Sci. Lett.*, *255*, 22–31.

Christensen, U. R., and A. W. Hofmann (1994), Segregation of subducted oceanic crust in the convecting mantle, *J. Geophys. Res.*, *99*, 19,867–19,884.

Cleary, J., and R. Haddon (1972), Seismic wave scattering near the core-mantle boundary: A new interpretation of precursors to PKP, *Nature*, *240*, 549–551.

Cormier, V. (2007), Texture of the uppermost inner core from forward- and back-scattered seismic waves, *Earth Planet. Sci. Lett.*, *258*, 442–453.

Crotwell, H., T. Owens, and J. Ritsema (1999), The TauP Toolkit: Flexible seismic travel-time and raypath utilities, *Seismol. Res. Lett.*, *70*, 154–160.

Deuss, A., J. Irving, and J. Woodhouse (2010), Regional variation of inner core anisotropy from seismic normal mode observations, *Science*, *328*, 1018–1020.

Doornbos, D. J. (1978), On seismic-wave scattering by a rough core-mantle boundary, *Geophys. J. R. Astron. Soc.*, *53*, 643–662.

Doornbos, D. J., and E. Husebye (1972), Array analysis of PKP phases and their precursors, *Phys. Earth Planet. Inter.*, *5*, 387–399.

Garnero, E., J. Revenaugh, Q. Williams, T. Lay, and L. Kellogg (1998), Ultralow velocity zone at the core mantle boundary, in *The Core-Mantle Boundary*, edited by M. Gurnis et al., pp. 319–334, AGU, Washington, D. C.

Garnero, E. J. (2000), Heterogeneity of the lowermost mantle, *Annu. Rev. Earth Planet. Sci.*, *28*, 509–537.

Goldstein, P., D. Dodge, M. Firpo, and L. Minner (2003), SAC2000: Signal processing and analysis tools for seismologists and engineers, in *The IASPEI International Handbook of Earthquake and Engineering Seismology*, edited by W. H. K. Lee et al., Academic Press, London.

Haddon, R., and J. Cleary (1973), A note on the interpretation of precursors to PKP, *Phys. Earth Planet. Inter.*, *7*, 495–497.

Hedlin, M., and P. Shearer (2000), An analysis of large-scale variations in small-scale mantle heterogeneity using Global Seismographic Network recordings of precursors to PKP, *J. Geophys. Res.*, *105*, 13,655–13,673.

Hedlin, M., P. Shearer, and P. Earle (1997), Seismic evidence for small-scale heterogeneity throughout the Earth's mantle, *Nature*, *387*, 145–150.

Kaneshima, S., and G. Helffrich (2009), Lower mantle scattering profiles and fabric below Pacific subduction zones, *Earth Planet. Sci. Lett.*, *282*, 234–239.

Koelemeijer, P., A. Deuss, and J. Trampert (2012), Normal mode sensitivity to Earth's D'' layer and topography on the core-mantle boundary: What we can and cannot see, *Geophys. J. Int.*, *190*, 553–568.

Li, C., R. van der Hilst, R. Engdahl, and S. Burdick (2008), A new global model for P wave speed variations in Earth's mantle, *Geochem. Geophys. Geosyst.*, *9*, Q05018, doi:10.1029/2007GC001806.

Mancinelli, N., and P. Shearer (2013), Reconciling discrepancies among estimates of small-scale mantle heterogeneity from PKP precursors, *Geophys. J. Int.*, *195*, 1721–1729.

Margerin, L., and G. Nolet (2003), Multiple scattering of high-frequency seismic waves in the deep Earth: PKP precursor analysis and inversion for mantle granularity, *J. Geophys. Res.*, *108*(B11), 2514, doi:10.1029/2003JB002455.

McNamara, A., E. Garnero, and S. Rost (2010), Tracking deep mantle reservoirs with ultra-low velocity zones, *Earth Planet. Sci. Lett.*, *299*, 1–9.

Miller, M., and F. Niu (2008), Bulldozing the core-mantle boundary: Localized seismic scatterers beneath the Caribbean Sea, *Phys. Earth Planet. Inter.*, *170*, 89–94.

Niu, F., and L. Wen (2001), Strong seismic scatterers near the core-mantle boundary west of Mexico, *Geophys. Res. Lett.*, *418*, 3557–3560.

Ritsema, J., H. van Heijst, and J. Woodhouse (2004), Global transition zone tomography, *J. Geophys. Res.*, *109*, B02302, doi:10.1029/2003JB002610.

Schimmel, M., and H. Paulssen (1997), Noise reduction and detection of weak, coherent signals through phase-weighted stacks, *Geophys. J. Int.*, *130*, 497–505.

Sigloch, K., and M. Mihalnyuk (2013), Intra-oceanic subduction shaped the assembly of Cordilleran North America, *Nature*, *496*, 50–56.

Sze, E., and R. van der Hilst (2003), Core mantle boundary topography from short period PcP, PKP, and PKKP data, *Phys. Earth Planet. Inter.*, *135*, 27–46.

Tanaka, S., and H. Hamaguchi (1997), Degree one heterogeneity and hemispherical variation of anisotropy in the inner core from PKP(BC)-PKP(DF) times, *J. Geophys. Res.*, *102*, 2925–2938.

Thomas, C., M. Weber, C. Wicks, and F. Scherbaum (1999), Small scatterers in the lower mantle observed at German broadband arrays, *J. Geophys. Res.*, *104*, 15,073–15,088.

Thomas, C., J. Kendall, and G. Helffrich (2009), Probing two low-velocity regions with PKP b-caustic amplitudes and scattering, *Geophys. J. Int.*, *178*, 503–512.

Vanacore, E., F. Niu, and Y. Ma (2010), Large angle reflection from a dipping structure recorded as a PKIKP precursor: Evidence for a low velocity zone at the core-mantle boundary beneath the Gulf of Mexico, *Earth Planet. Sci. Lett.*, *293*, 54–62.

Vidale, J., and M. Hedlin (1998), Evidence for partial melt at the core-mantle boundary north of Tonga from the strong scattering of seismic waves, *Nature*, *391*, 682–685.

Waszek, L., and A. Deuss (2011), Distinct layering in the hemispherical seismic velocity structure of Earth's upper inner core, *J. Geophys. Res.*, *116*, B12313, doi:10.1029/2011JB008650.

Waszek, L., and A. Deuss (2013), A low attenuation layer in Earth's uppermost inner core, *Geophys. J. Int.*, *195*, 2005–2015.

Waszek, L., J. Irving, and A. Deuss (2011), Reconciling the hemispherical structure of Earth's inner core with its super-rotation, *Nat. Geosci.*, *4*, 264–267.

Wen, L. (2000), Intense seismic scattering near the Earth's core-mantle boundary beneath the Comoros hotspot, *Geophys. Res. Lett.*, *27*, 3627–3630.

Wen, L., and D. Helmberger (1998), Ultra-low velocity zones near the core-mantle boundary from broadband PKP precursors, *Science*, *279*, 1701–1703.

Wen, L., and F. Niu (2002), Seismic velocity and attenuation structures in the top of the Earth's inner core, *J. Geophys. Res.*, *107*(B11), 2273, doi:10.1029/2001JB000170.

Yee, T., J. Rhie, and H. Tkalčić (2014), Regionally heterogeneous uppermost inner core observed with Hi-net array, *J. Geophys. Res. Solid Earth*, *119*, 7823–7845, doi:10.1002/2014JB011341.